AIP | The Journal of Chemical Physics

Scaling between relaxation, transport and caged dynamics in a binary mixture on a per-component basis

F. Puosi, C. De Michele, and D. Leporini

Citation: J. Chem. Phys. **138**, 12A532 (2013); doi: 10.1063/1.4789943
View online: http://dx.doi.org/10.1063/1.4789943
View Table of Contents: http://jcp.aip.org/resource/1/JCPSA6/v138/i12
Published by the American Institute of Physics.

Scaling between relaxation, transport and caged dynamics in a binary mixture on a per-component basis

F. Puosi,[1] C. De Michele,[2] and D. Leporini[1,3,a)]
[1]*Dipartimento di Fisica "Enrico Fermi," Università di Pisa, Largo B. Pontecorvo 3, I-56127 Pisa, Italy*
[2]*Dipartimento di Fisica, "Sapienza" Università di Roma, Piazzale Aldo Moro 2, 00185 Roma, Italy*
[3]*IPCF-CNR, UOS Pisa, Italy*

(Received 28 September 2012; accepted 17 January 2013; published online 7 February 2013)

The universal scaling between the *average* slow relaxation/transport and the *average* picosecond rattling motion inside the cage of the first neighbors has been evidenced in a variety of numerical simulations and experiments. Here, we first show that the scaling does not need information concerning the arbitrarily-defined glass transition region and relies on a single characteristic length scale $\overline{a^2}^{1/2}$ which is determined even *far* from that region. This prompts the definition of a novel reduced rattling amplitude $\widehat{\langle u^2\rangle}^{1/2}$ which has been investigated by extensive molecular-dynamics simulations addressing the slow relaxation, the diffusivity, and the fast cage-dynamics of both components of an atomic binary mixture. States with different potential, density, and temperature are considered. It is found that if two states exhibit coinciding incoherent van Hove function on the picosecond timescale, the coincidence is observed at long times too, including the large-distance exponential decay—a signature of heterogeneous dynamics—observed when the relaxation is slow. A major result of the present study is that the correlation plot between the diffusivity of the two components of the binary mixtures and their respective reduced rattling amplitude collapse on the same master curve. This holds true also for the structural relaxation of the two components and the unique master curve coincides with the one of the *average* scaling. It is shown that the breakdown of the Stokes-Einstein law exhibited by the distinct atomic species of the mixture and the monomers of a chain in a polymer melt is predicted at the *same* reduced rattling amplitude. Finally, we evidence that the well-known temperature/density thermodynamic scaling of the transport and the relaxation of the mixture is still valid on the picosecond timescale of the rattling motion inside the cage. This provides a link between the fast dynamics and the thermodynamic scaling of the slow dynamics. © *2013 American Institute of Physics*. [http://dx.doi.org/10.1063/1.4789943]

I. INTRODUCTION

Understanding the progressive solidification of a liquid to get to the amorphous glassy state is a major scientific challenge.[1–4] On approaching the glass transition, particles are trapped by the cage of the first neighbors more effectively and the average escape time, i.e., the structural relaxation time τ_α increases from a few picoseconds up to thousands of seconds. The caged particles are not completely immobilized by the surroundings but they wiggle with mean-square amplitude $\langle u^2\rangle$ on the picosecond time scale $t^\star$.[5] Henceforth, $\langle u^2\rangle$ will be referred to as short-time mean-square displacement (ST-MSD). Despite the huge range of time scales older[6] and recent theoretical[7–13] studies addressed the underlying rattling process to understand the structural relaxation gaining support from numerical[13–23] and experimental works on glassforming liquids[13,24,65] and glasses[10,25–30] (for a review see Ref. 31).

In recent papers extensive molecular-dynamics (MD) simulations evidencing the universal correlation between the structural relaxation time τ_α and $\langle u^2\rangle$ were reported.[32,33] The master curve is accounted for by the analytical form

$$\tau_\alpha = \tau_0 \exp\left(\frac{\overline{a^2}}{2\langle u^2\rangle} + \frac{\sigma_{a^2}^2}{8\langle u^2\rangle^2}\right). \quad (1)$$

$\overline{a^2}$ and $\sigma_{a^2}^2$ are the average and the variance of the truncated gaussian distribution of the square displacements to overcome the energy barriers, respectively, with ratio (see the Appendix)

$$\frac{\sigma_{a^2}}{\overline{a^2}} = \Lambda = 2.015(1). \quad (2)$$

In order to compare Eq. (1) with the available experimental data one needs suitable reduced ST-MSD. To this aim, in Refs. 32 and 33, $\langle u^2\rangle$ has been rescaled by its value $\langle u_g^2\rangle$ at the glass transition (defined as the state where $\tau_\alpha = 10^2$ s or alternatively the viscosity $\eta = 10^{12}$ Pa s). This recasts Eq. (1) in a universal form with only *one* adjustable parameter, i.e., the conversion factor τ_{CF} to convert τ_0 in MD units to the corresponding quantity in actual time units (if viscosity data are used, the factor is named η_{CF}). The conversion factors little depend on the system (with the notable exception of B_2O_3).[32–34]

Actually, *if the scaling is genuine*, instead of $\langle u_g^2\rangle^{1/2}$, any other choice of the characteristic length scale, say λ, to define

a)Electronic mail: dino.leporini@df.unipi.it.

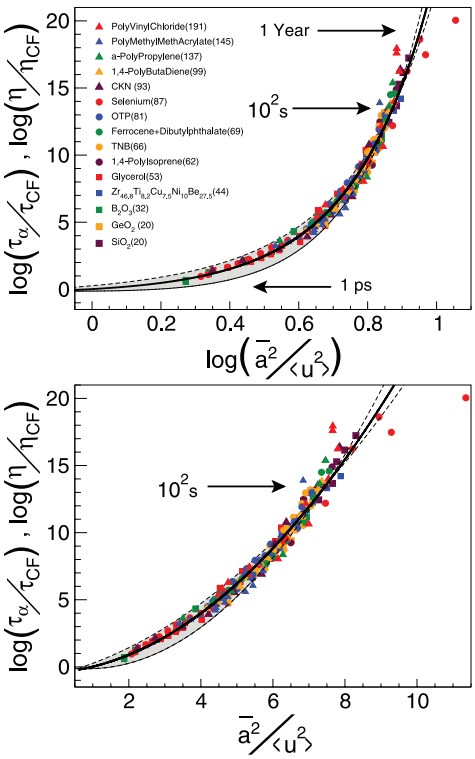

FIG. 1. Log-log (top) and log-linear (bottom) plots of the reduced relaxation time and viscosity vs. the reduced cage-rattling amplitude. τ_{CF} and η_{CF} are the conversion factors from the MD time or viscosity units to the actual units, respectively. The two panels emphasize the fast (top) and the slow (bottom) relaxation regimes. The numbers in parenthesis denote the fragility m. The black curve is Eq. (3). The dashed curves bound the accuracy of the scaling.[32] Experimental details are given elsewhere.[35] For each glassformer $\overline{a^2}$ is drawn by fitting Eq. (1) to the experimental data τ_α (or η) vs. $1/\langle u^2\rangle$ with Eq. (2) as constraint and considering τ_{CF}, or η_{CF}, as adjustable. The conversion factors little depend on the system (with the notable exception of B_2O_3).[32–34]

the reduced ST-MSD $\widehat{\langle u_i^2\rangle} = \langle u_i^2\rangle/\lambda^2$ is acceptable and leads to a universal curve. A convenient choice for both the experimental and the numerical work is to set $\lambda = \overline{a^2}^{1/2}$, a value which is readily drawn by fitting Eq. (1) to the unscaled data τ_α (or η) vs. $\langle u^2\rangle$ with Eq. (2) as constraint, and *no* resort to information on the glass transition (and even no need to approach it). This recasts the master curve, Eq. (1), as

$$\tau_\alpha = \tau_0 \exp\left(\frac{1}{2}\frac{1}{\widehat{\langle u^2\rangle}} + \frac{\Lambda^2}{8}\frac{1}{\widehat{\langle u^2\rangle}^2}\right) \tag{3}$$

in terms of the reduced ST-MSD:

$$\widehat{\langle u^2\rangle} = \frac{\langle u^2\rangle}{\overline{a^2}}. \tag{4}$$

All in all, the novel scaling procedure needs the adjustment of two parameters, $\overline{a^2}$ and τ_{CF} (or η_{CF}), whereas the original one sets $\lambda = \langle u_g^2\rangle^{1/2}$ and adjusts τ_{CF} (or η_{CF}) only.[32,33] The master curve Eq. (3) fits with the existing experimental data from supercooled liquids, polymers, ionic liquids, and metallic glasses over about eighteen decades of relaxation times and a very wide range of fragilities (Fig. 1). It is interesting to note that since $\langle u_g^2\rangle$ is largely uncorrelated with the fragility,[33] the same applies to $\overline{a^2}$ due to their close relation.[36]

In addition to the above systems, the scaling has been also evidenced in simulations of atomic liquids,[33] antiplasticized polymers,[13] and colloidal gels, the latter being *very diluted* systems.[37] More recently, the influence of free volume and the proper time scales to observe the genuine fast dynamics have been considered[34,35] as well as the breakdown of the Stokes-Einstein (SE) law,[38] the relation with the elastic modulus,[39] and the spatial extension of the involved particle displacements at short-times.[40] Simmons *et al.* derived an expression of the master curve between τ_α and ST-MSD with three adjustable parameters accounting for the anisotropic nature of particle localization.[13] The latter master curve is compared with Eq. (1) elsewhere.[41] A related remark is given in Sec. IV C 4.

Equations (1) and (3) provide a vivid, easy-to-grasp way to convey the correlation between the picosecond and the ultraslow dynamics. However, more fundamental insight into the scaling is provided by the incoherent, or self part, of the van Hove function $G_s(\mathbf{r}, t)$.[42,43] The interpretation of $G_s(r, t)$ is direct. The product $G_s(r, t) \cdot 4\pi r^2\, dr$ is the probability that the particle is at a distance between r and $r + dr$ from the initial position after a time t. In terms of the incoherent van Hove function the scaling property is expressed by stating that if two physical states, say X and Y, are characterized by the *same* self part of the van Hove function $G_s(\mathbf{r}, t^\star)$ at the characteristic rattling time $t^\star$, they also exhibit the *same* self part of the van Hove function at long times[44]

$$G_s^{(X)}(\mathbf{r}, t^\star) = G_s^{(Y)}(\mathbf{r}, t^\star) \iff G_s^{(X)}(\mathbf{r}, \tau_\alpha) = G_s^{(Y)}(\mathbf{r}, \tau_\alpha). \tag{5}$$

Equation (5) is by no means obvious and was shown to hold even in the presence of very strong dynamical heterogeneity[4,45] where both diffusive and jump-like dynamics are observed in different spatial regions over times comparable with τ_α.[44] In this respect, Eq. (5) supports previous conclusions that the long-time dynamical heterogeneity is predicted by the fast heterogeneities.[19,46]

Recently, some of the present authors considered physical states of a polymer melt with marked dynamical heterogeneity and fulfilling Eq. (5), i.e., with equal τ_α.[40] It was found that the particles belonging to the "fast" and the "slow" components of these states exhibit the same spatial correlation of the displacements of their surroundings within both $t^\star$ and τ_α. This is a first piece of evidence that the correlation between the fast and the slow dynamics is not only observed in terms of *global* averages but holds for *specific* dynamical subsets too. The present paper is motivated by pursuing a better understanding of this issue. To this aim, we consider the case of the atomic binary mixtures where the two components of atoms, say A and B, identify two distinct dynamical subsets in a natural way. It is known that atomic binary mixtures comply with the scaling between the average slow relaxation/transport and the average picosecond rattling motion inside the cage of the first neighbors.[33]

The paper is organized as follows. In Sec. II details about the numerical simulations are given. In Sec. III the quantities of interest are defined. The results are presented and discussed in Sec. IV and the main conclusions are summarized in Sec. V.

II. NUMERICAL METHODS

An 80:20 binary mixture of $N_{bm} = 1000$ particles is considered. The two species are labelled A and B and particles interact via the potential

$$U_{q,p,\alpha,\beta}(r) = \frac{\epsilon_{\alpha,\beta}}{q-p}\left[p\left(\frac{\sigma^*_{\alpha,\beta}}{r}\right)^q - q\left(\frac{\sigma^*_{\alpha,\beta}}{r}\right)^p\right] + U_{cut}, \tag{6}$$

where $\sigma^*_{\alpha,\beta} = 2^{1/6}\sigma_{\alpha,\beta}$ is the position of the minimum of the potential with depth $\epsilon_{\alpha,\beta}$. The value of the constant U_{cut} is chosen to ensure $U_{q,p}(r) = 0$ at $r \geq r_c = 2.5\,\sigma$. The well height and the minimum of the potential depend on the interacting species, being $\alpha, \beta \in A, B$ with $\sigma_{AA} = 1.0$, $\sigma_{AB} = 0.8$, $\sigma_{BB} = 0.88$, $\epsilon_{AA} = 1.0$, $\epsilon_{AB} = 1.5$, $\epsilon_{BB} = 0.5$, and $m_A = m_B = 1$. For a given pair (α, β), changing the parameters p and q does not affect the position $r = \sigma^*_{\alpha,\beta}$ or the depth $\epsilon_{\alpha,\beta}$ of the potential minimum but only the steepness of the repulsive and the attractive wings. Note that setting $q = 12$ and $p = 6$ in Eq. (6) and the above choices for $\sigma_{\alpha,\beta}$ and $\epsilon_{\alpha,\beta}$ reduces the model to the well-known Lennard-Jones Kob-Andersen model.[48–50] Using argon units for the A-particles, i.e., $\epsilon_{AA}/k_B = 119.8$ K, $\sigma_{AA} = 0.3405$ nm, $m_A = 6.6337 \times 10^{-26}$ kg, the time unit is $\tau'_{MD} = (\sigma^2_{AA} m_A/\epsilon_{AA})^{1/2} = 2.2$ ps.[51] The system was equilibrated in the NTV ensemble and the production runs were carried out in the NVE ensemble (NVT: constant number of particles, volume and temperature; NVE: constant number of particles, volume and energy). NTV runs using a standard Nosé method.[52] The "velocity verlet" integration algorithm was used both in the NVE and NTV ensembles.[53]

We investigate states with different number density ρ, temperature T, and interacting potential $U_{q,p,\alpha,\beta}(r)$, as specified by the (p, q) pair. For clarity reasons, the details about the states, each denoted by the list (ρ, T, p, q), are given in the captions of the figures.

III. VAN HOVE FUNCTION AND RELATED QUANTITIES

Our quantities of interest are strictly related to the self part of the van Hove function $G_s(\mathbf{r}, t)$,[43]

$$G_s(\mathbf{r}, t) = \frac{1}{N}\left\langle \sum_{i=1}^{N} \delta[\mathbf{r} + \mathbf{r}_i(0) - \mathbf{r}_i(t)] \right\rangle, \tag{7}$$

where $\boldsymbol{r}_i(t)$ is the position of the ith particle at time t. In isotropic liquids the van Hove function depends on the modulus r of $\mathbf{r}$. The moments of $G_s(r, t)$ are of interest

$$\langle r^n(t)\rangle = 4\pi \int_0^\infty r^n G_s(r, t)\, r^2 dr \tag{8}$$

or alternatively

$$\langle r^n(t)\rangle = \frac{1}{N}\sum_i \langle \|\mathbf{r}_i(t) - \mathbf{r}_i(0)\|^n \rangle. \tag{9}$$

For $n = 2$ one recovers the usual mean square displacement. In the ballistic regime $\langle r^2(t)\rangle = 3k_BT/m\,t^2$, whereas at very long times $\langle r^2(t)\rangle = 6Dt$, where D is the diffusion coefficient.

The spatial Fourier transform of the self part of the van Hove function yields the self part of the intermediate scattering function (ISF)[43]

$$F_s(\boldsymbol{q}, t) = \int G_s(\boldsymbol{r}, t)\exp(-i\boldsymbol{q}\cdot\boldsymbol{r})\, d\boldsymbol{r} \tag{10}$$

which in an isotropic liquid depends only on the modulus of the wavevector $q = ||\boldsymbol{q}||$ and is expressed as

$$F_s(q, t) = \frac{1}{N}\left\langle \sum_j^N e^{i\mathbf{q}\cdot(\mathbf{r}_j(t) - \mathbf{r}_j(0))} \right\rangle. \tag{11}$$

ISF provides a convenient function to study the rearrangements of the spatial structure of the fluid over the length scale $\sim 2\pi/q$. We consider q values corresponding to the maxima of the static structure factors of each component, S_{AA} and S_{BB}. For A particles, $2\pi/q^{(A)}_{max} \sim 0.86\sigma_{AA}$, i.e., we investigate the cage of one A particle due to, mostly, other A particles. For B particles, $2\pi/q^{(B)}_{max}$ is about the average BB interparticle distance $\bar{r}_{BB} \sim 1.1\sigma_{AA}$. We define the structural relaxation times of the A and B components by the relation $F_s(q^{(i)}_{max}, \tau_{\alpha\,i}) = 1/e$ with $i = A, B$.

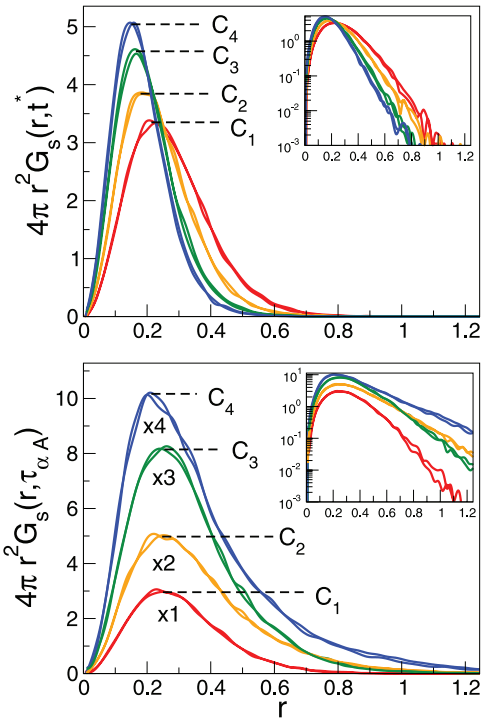

FIG. 2. Self-part of the Van Hove function of the A particles $G_s(r, t^\star)$ (top) and $G_s(r, \tau_{\alpha A})$ (bottom) in selected states (ρ, T, p, q) (p and q are the characteristic exponents of the potential Eq. (6)). Note that states with identical $G_s(r, t^\star)$ have identical $G_s(r, \tau_{\alpha A})$, Eq. (5). The same correlation has been noted in polymers.[44] The clusters of states (ρ, T, p, q) are: C_1 cluster: (1.204,1.0,6, 12), (1.204, 0.5,5,8) with $\tau_{\alpha A} \simeq 1.2$; C_2 cluster: (1.204, 0.6,6, 12), (1.125, 0.425, 6, 12) with $\tau_{\alpha A} \simeq 4.7$; C_3 cluster: (1.125, 0.525,6, 12), (1.063,0.45,6, 12) with $\tau_{\alpha A} \simeq 15$; C_4 cluster: (1.204,0.27,5,8), (1.204, 0.481,6,11) with $\tau_{\alpha A} \simeq 62$. (Inset): tails of $G_s(r, t^\star)$ (top) and $G_s(r, \tau_{\alpha A})$ (bottom). Note the developing exponential decay at large distances on increasing $\tau_{\alpha A}$, a signature of dynamic heterogeneity.[47] The exponential tail of $G_s(r, t)$ is observed at both short ($t = t^\star$, top panel) and long ($t = t^\star$, bottom panel) times.

IV. RESULTS AND DISCUSSION

A. Relaxation and transport

Figure 2 shows that the incoherent van Hove function of the component A of the binary mixture fulfills Eq. (5), namely, if two states exhibit coinciding incoherent van Hove function on the picosecond timescale, the coincidence is observed at long times too. In particular, the coincidence is seen at large distances where the tails of both $G_s(r, t^\star)$ and $G_s(r, \tau_{\alpha A})$ decay exponentially in the case of slowly relaxing states (see inset of Fig. 2). The fact that the tails of the distributions exhibit exponential, rather than Gaussian, decay is considered a universal manifestation of the the coexistence of slow and fast particles (dynamic heterogeneity[4,45]).[47] From this respect, it is remarkable that the coincidence of the particle dynamics on the picosecond timescale ensures the coincidence of the van Hove function $G_s(r, \tau_{\alpha A})$ at large distances too, thus suggesting that long-time dynamic heterogeneity is encoded at short times.[19,46] The issue will be discussed in Secs. IV C 3 and IV C 4.

Figure 3 shows typical MSD and ISF curves of the A and B particles. At very short times (ballistic regime) MSD increases according to $\langle r^2(t)\rangle \cong (3k_BT/m)t^2$ and ISF starts to decay. The repeated collisions with the other particles slow the displacement of the tagged one. At later times a quasi-plateau region, also found in ISF, develops when the temperature is lowered and/or the density increased. This signals the increased stability of the structure on the length scale $2\pi/q_{max}$. For $t \gtrsim \tau_\alpha$ the structure relaxes and the subsequent motion is diffusive, $\langle r^2(t)\rangle = 6Dt$ with D the diffusion coefficient. A and B particles exhibit distinct diffusion coefficients D_A and D_B, respectively ($D_B > D_A$).

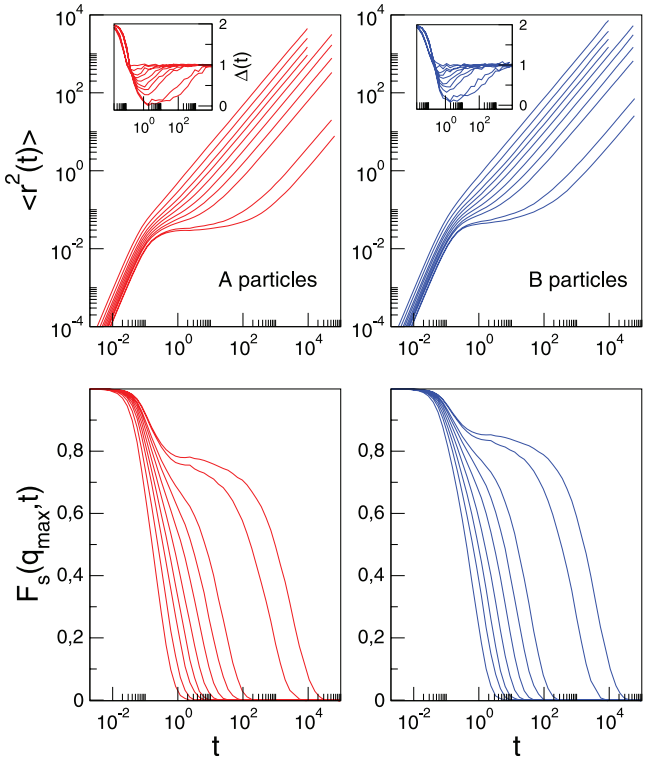

FIG. 3. (Top) MSD of the A (left) and B (right) particles in selected states (ρ, T, p, q). (Inset) Plot of $\Delta(t) \equiv \partial\log\langle r^2(t)\rangle/\partial\log t$. The minimum of $\Delta(t)$ occurs at the time $t^\star$, a measure of the trapping time of the particle ($t^\star$ is the same for A and B particles within the errors). (Bottom) Corresponding ISF functions. The q_{max} values for the particles A and the B are $q^{(A)}_{max} \sim 2\pi/\sigma_{AA}$ and $q^{(B)}_{max} \sim 2\pi/\bar{r}_{BB}$, where $\bar{r}_{BB}$ is the average distance between B particles. The plotted states have parameters $\rho = 1.204$, $T = 0.45$, 0, 48, 0.6, 0.7, 0.8, 1.0, 1.2, 1.5, 2.0, 3.0 (from the rightmost to the leftmost curve in each panel) and Lennard-Jones interacting potential (Eq. (6) with $p = 6$, $q = 12$).

B. Heterogeneous dynamics

The states considered in Fig. 3 exhibit heterogeneous dynamics, i.e., a spatial distribution of mobility.[4] The magnitude of the deviation from the homogeneous dynamics is usually quantified by the deviations from the gaussian character of the displacement and is expressed by the non-gaussian parameter,

$$\alpha_2(t) = \frac{3}{5}\frac{\langle r^4(t)\rangle}{\langle r^2(t)\rangle^2} - 1. \tag{12}$$

For gaussian variables α_2 vanishes. Figure 4 plots the non-gaussian parameter for all the states considered in Fig. 3. Deviations from the gaussian behaviour, usually ascribed to more prominent jump-like dynamics, first increase with time and then decay in the diffusive gaussian regime, resulting in a maximum α_2^{max}. The smaller B particles exhibit stronger heterogeneous dynamics than the A particles, suggesting that they jump more easily. Non-gaussianity increases by decreasing the temperature.

C. Scaling of relaxation and transport in terms of the caged dynamics

1. Picosecond mean square displacement

In order to characterize the cage fast dynamics we consider the MSD evaluated at a characteristic time scale $t^\star$ which is defined by the condition that the derivative $\Delta(t) \equiv \partial\log\langle r^2(t)\rangle/\partial\log t$ is minimum at $t^\star$, i.e., $t^\star$ is the time when MSD changes the concavity in the log-log plot.[32,33] $t^\star$ is a measure of the trapping time of the particle. In actual units it corresponds to a few picoseconds. The plots of $\Delta(t)$ in Fig. 3 (inset) show that $t^\star$ for the present binary mixtures increases slightly with the structural relaxation time, while it was found to be virtually constant in a polymer melt.[33]

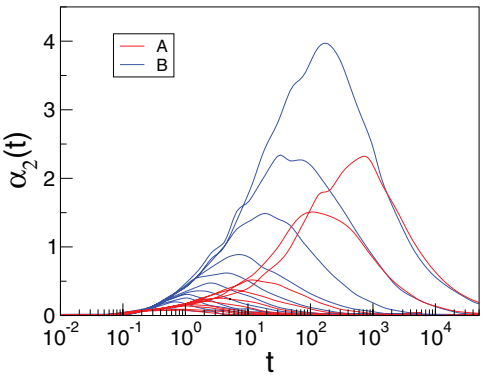

FIG. 4. Non-gaussian parameter of the states in Fig. 3. Heterogeneous dynamics develops as time goes by and decays at long times in the diffusive regime, resulting in a maximum value of the parameter α_2^{max}. Non-gaussianity increases by decreasing the temperature.

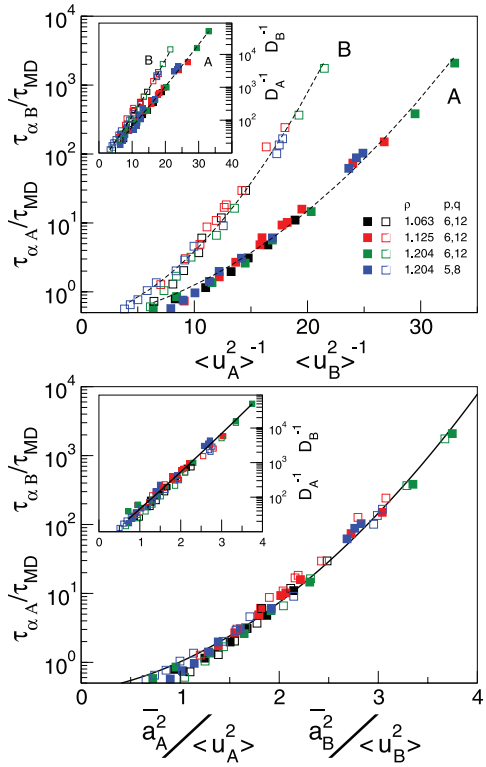

FIG. 5. (Top) Correlation plot between the structural relaxation times, the diffusivity (inset), and the picosecond MSD of the components A and B. The dashed lines in the main panel are best-fits with Eq. (1) and parameters as Table I. The dashed lines in the inset are (virtually linear) guides for the eyes. (Bottom) Scaling of the master curves of the A and B components. The black solid line is Eq. (3). The latter, as Eq. (1),[32,33] fails for $\tau_\alpha \lesssim 1$. The black solid line in the inset is a (virtually linear) guide for the eyes. The plotted states are: (i) all the states in Fig. 3; (ii) states with interacting potential $U_{5,\,8,\,\alpha,\,\beta}(r)$, $\rho = 1.204$, T = 0.267, 0.270, 0.275, 0.350, 0.400, 0.450, 0.500, 0.600, 0.700, 0.800, 0.900, 1.000, 1.200, 1.500, 2.000, 3.000; (iii) states with LJ interacting potential $U_{6,\,12,\,\alpha,\,\beta}(r)$, $\rho = 1.125$ with T = 0.350, 0.375, 0.425, 0.450, 0.475, 0.500, 0.525, 0.600, 0.700, 1.000, 2.000, 3.000 and $\rho = 1.063$ with T = 0.35, 0.4, 0.45, 0.5, 0.6, 0.7, 1.0, 2.0, 3.0.

We are now in a position to define the picosecond ST-MSD as[32,33]

$$\langle u^2 \rangle \equiv \langle r^2(t = t^\star) \rangle. \tag{13}$$

At high temperature the cage picture loses its significance, as signaled by the disappearance of the inflection point in the log-log plot of the MSD time-dependence (Fig. 3, inset). This limits the applicability range of both the definition of $\langle u^2 \rangle$ and Eqs. (1) and (3).

2. Relaxation and transport

Figure 5 (top) shows the correlation plots of the ST-MSD with both the structural relaxation time and the diffusion coefficient of both components of the binary mixture. The superimposed master curves, which are fits with Eq. (1) with parameters as in Table I, show that A and B subsets obey Eq. (2). The master curves of the two components are collapsed to a single master curve with distinct forms for τ_α and D by considering the reduced ST-MSD $\widehat{\langle u_i^2 \rangle}$, $i = A, B$, Eq. (4). The master curve for τ_α is Eq. (3). Expectedly, Eq. (3), as Eq. (1),[32,33] fails for $\tau_\alpha \lesssim 1$, since the cage picture loses its significance, as signaled by the disappearance of the inflection point in the MSD vs. time log-log plot (see Fig. 3).

TABLE I. Parameters of Eq. (1) for the A and B particles of the binary mixture of the present study ($i = A, B$) and the polymer melt characterized previously ($i = P$).[32,33,38–40,44] Note that both the A and B subsets of the mixture and the polymer obey Eq. (2).

	$\overline{a_i^2}$	$\sigma_{a_i^2}$	$\sigma_{a_i^2}/\overline{a_i^2}$
A	0.1124	0.2264	2.014
B	0.1706	0.3438	2.015
P	0.1243	0.2506	2.016

Noticeably, it is found that within the errors

$$\sqrt{\frac{\overline{a_A^2}}{\overline{a_B^2}}} = 0.811 \simeq \frac{\sigma^*_{AB}}{\sigma^*_{AA}}, \tag{14}$$

where $\sigma^*_{\alpha\beta}$ is the equilibrium distance between α and β particles, see Sec. II. More work is needed to put Eq. (14) on a firmer ground. At this level, it is enough to note that the above relation does not involve the length scale σ^*_{BB}, most probably due to the fact that the B particles are mostly surrounded by A particles, as well as the ratio of the two energy scales potentially involved, $\epsilon_{AB}/\epsilon_{AA} = 1.5$.

Interestingly, the scaling curves for the diffusion coefficients are virtually linear in $1/\langle u^2 \rangle$, i.e., $\log D \propto 1/\langle u^2 \rangle$. A tentative explanation relies on the finding that the deviation from the linearity in Eq. (1) for τ_α increases with the dynamic heterogeneity (see Refs. 32 and 38 and Sec. IV C 3). In fact, the latter affects the gaussian character of the displacement much more effectively at time $t \sim \tau_\alpha$ than in the diffusive regime at $t \gg \tau_\alpha$ (see Fig. 4).

3. Heterogeneous dynamics

Figure 6 plots the maximum of the non-gaussian parameters of the two components, α_{2A}^{max} and α_{2B}^{max}, in terms of the corresponding reduced ST-MSD $\widehat{\langle u_A^2 \rangle}$ and $\widehat{\langle u_B^2 \rangle}$. It is seen that

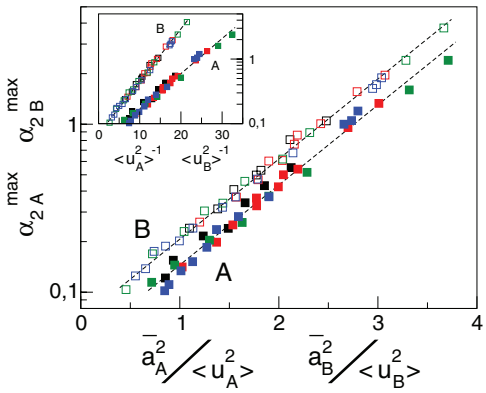

FIG. 6. Scaling of the non-gaussian parameters of the components A and B for all the states of Fig. 5 in terms of the reduced ST-MSD $\widehat{\langle u_i^2 \rangle}$, $i = A, B$, Eq. (4). The two dashed lines are parallel. The inset shows that parallelism is lost by using the ST-MSD.

if $\widehat{\langle u_i^2 \rangle}$ is small, then: (i) the right-hand side of Eq. (3) reduces to the original form proposed long time ago[8,24] and (ii) α_2^{max} is small, i.e., the particle displacement is nearly gaussian. It is also seen that α_2^{max} increases exponentially with $\widehat{\langle u_i^2 \rangle}^{-1}$. The same conclusions were also drawn from a model polymer system.[32,33] A brownian model of the cage dynamics predicts a much weaker linear dependence between α_2^{max} and $\widehat{\langle u_i^2 \rangle}^{-1}$.[54]

Notably, the slope of $\log \alpha_{2i}^{max}$ vs. $\widehat{\langle u_i^2 \rangle}$ is the same for A and B particles, whereas this is not the case if one uses the ST-MSD. This shows that the reduced ST-MSD removes part of the differences concerning the dynamical heterogeneity of the two kind of particles (see inset of Fig. 6). This aspect is further investigated in Subsection IV C 4 devoted to the breakdown of the Stokes-Einstein law.

4. Stokes-Einstein law

We focus on the SE law which for a sphere with radius a and stick boundary conditions reads

$$D = k_B T/(6\pi\, a\, \eta), \tag{15}$$

where D, k_B, T are the translational diffusion coefficient, Boltzmann's constant, and temperature, respectively. We assume $\tau_\alpha \propto \eta/T$ in accordance with numerical results[56] and experiments on glassforming systems[57] and study the product $D\tau_\alpha$ for each component of the mixture. The results, which are shown in Fig. 7, provide evidence that in the highly fluid states (small α_2^{max} and reduced ST-MSD values) the product $D\,\tau_\alpha$ is—as predicted by the SE law[56,57]—nearly constant, whereas for highly viscous states the mobility is higher than expected from the SE law due to dynamical heterogeneity.[4,45,58] Notice that the SE breakdown occurs when the second term on the right hand side of Eq. (3) becomes larger than the first term.

States with equal α_2^{max} or reduced ST-MSD exhibit nearly equal values of the product $D\,\tau_\alpha$ within the errors suggesting that both quantities (namely α_2^{max} and reduced ST-MSD) can be equally used to check the SE validity. Even if this is well-known for α_2^{max} which is associated to the *long-time* dynamics, it is by no means obvious for the reduced ST-MSD which is evaluated at $t^\star$, corresponding to a few picoseconds. The finding supports previous conclusions that the long-time dynamical heterogeneity is predicted by the fast dynamics.[19,46]

We now discuss the characteristic value of the reduced ST-MSD where the SE law breaks down. Figure 7 shows that the SE fails if

$$1/\widehat{\langle u_i^2 \rangle} > 1.9(1), \quad i = A, B, P \tag{16}$$

for both the atomic mixture ($i = A, B$) and a model polymer system ($i = P$).[38,55] Differently, the values of the non-gaussian parameter marking the onset of the SE violation of the A and B particles are somewhat different. By combining Eq. (16) with Eq. (2), one finds that SE is violated if ST-MSD obeys the inequality

$$\langle u_i^2 \rangle \lesssim 0.26\, \sigma_{a_i^2}, \quad i = A, B, P. \tag{17}$$

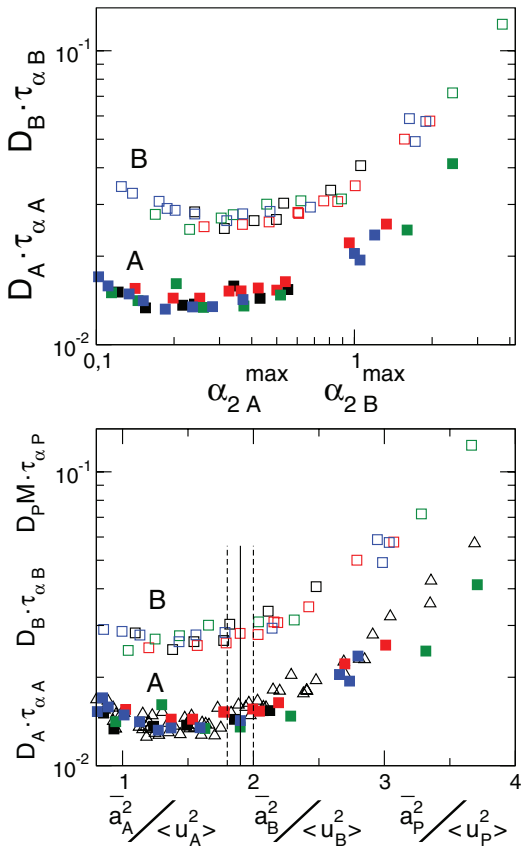

FIG. 7. The product $D_i\,\tau_{\alpha\,i}$ vs. α_{2i}^{max} (top panel) and the reduced ST-MSD $\widehat{\langle u_i^2 \rangle}$ (bottom panel), $i = A, B$ for all the states of Fig. 5. The onset of the SE violation for $1/\widehat{\langle u_i^2 \rangle} > 1.9(1)$ is indicated with the full vertical lines (uncertainty marked by dashed lines). Notice that the SE breakdown occurs when the second term on the rhs of Eq. (3) becomes larger than the first term. The bottom panel also plots the quantity $D_P M\,\tau_{\alpha\,P}$ vs. $\widehat{\langle u_P^2 \rangle}$ (empty triangles), referring to a model polymer system with chain length M, and shows that the SE breakdown occurs at the same point.[38,55]

Notably, the same inequality holds in two systems as different as an atomic mixture and a polymer melt. The inequality shows that SE is violated if the picosecond mean square displacement of the trapped monomer is smaller than the breadth of the distribution of the square displacements to get away from the cage of the first-neighbors. As a consequence, one anticipates that the distribution of the escape rates widens by decreasing $\langle u^2 \rangle$, i.e., increasing τ_α, thus yielding the coexistence of trapped and mobile particles, i.e., the dynamic heterogeneity.[4,45,58]

If inequality (16) holds, the SE law fails (Fig. 7) and the dynamic heterogeneity is apparent (Fig. 6). In this case the second term on the rhs of Eq. (3) becomes larger than the first term (they are equal if $1/\widehat{\langle u_i^2 \rangle} = 1$). The fact that Eq. (3) predicts a crossover from a dynamically homogeneous regime, where $\ln \tau_\alpha \propto 1/\widehat{\langle u^2 \rangle}$, to a heterogeneous one, where $\ln \tau_\alpha \propto 1/\widehat{\langle u^2 \rangle}^2$ is a distinctive feature of our model. Differently, in the localization model by Simmons *et al.* the master curve takes the form[13]

$$\tau_\alpha = \tau_0 \exp\left[\left(u_0^2/\langle u^2 \rangle\right)^{\alpha/2}\right], \tag{18}$$

where τ_0, u_0, and α are system-dependent adjustable parameters ($\alpha \sim 3-5$). On cooling from equilibrium to deeply supercooled states, $\langle u^2 \rangle$ decreases. However, Eq. (18) does not exhibit in a natural way either a crossover from a dynamically homogeneous regime to a heterogeneous one or other signatures of the increasing role played by the dynamic heterogeneity.

As a final remark, we note that the SE breakdown occurs at $\tau_\alpha \sim 10$–20 in MD units, corresponding to $\sim$20–40 ps, i.e., at much shorter relaxation times than the real systems where it occurs in the nanosecond range.[45] This fact was already noted.[59]

5. Thermodynamics scaling

In recent years much effort has been devoted to investigate the phenomenon of the glass transition by using the hydrostatic pressure as an experimental variable in addition to the temperature (for a review see Ref. 60). Several studies reported that the structural relaxation time, as well as other quantities like the diffusion coefficient, can be expressed as a function of the reduced quantity ρ^γ/T, e.g., $\tau_\alpha = \Im_{\tau_\alpha}(\rho^\gamma/T)$, where γ and $\Im$ are material-specific and $\Im_X$ depends on the specific dynamic process X too.[60] This scaling procedure of relaxation times is often referred to as "thermodynamic scaling."

Figure 8 shows that the thermodynamic scaling holds for both the structural relaxation and the diffusivity, as already known for binary mixtures.[61,62] In addition, Fig. 8 (top) shows that the thermodynamic scaling holds for ST-MSD as in ionic liquids[63] and polymers.[64]

The thermodynamic scaling of the structural relaxation is related to the scaling of ST-MSD. To show that, we fit the curve $\langle u_A^2 \rangle^{1/2}$ vs. ρ^γ/T in Fig. 8 (top) with a polynomial. The best-fit curve is used as input in Eq. (1) with $\overline{a_A^2}$ and $\sigma_{a_A^2}$ as in Table I to get an expression, with no adjustable parameter, of the master curve τ_α vs. ρ^γ/T. The result is shown in Fig. 8 (middle) and proves that the picosecond dynamics offers a route to interpret the thermodynamics scaling. The deviations of the master curve from the results concerning the fast-relaxing states are ascribed to the failure of Eq. (1) for relaxation times shorter than 1.[32,33]

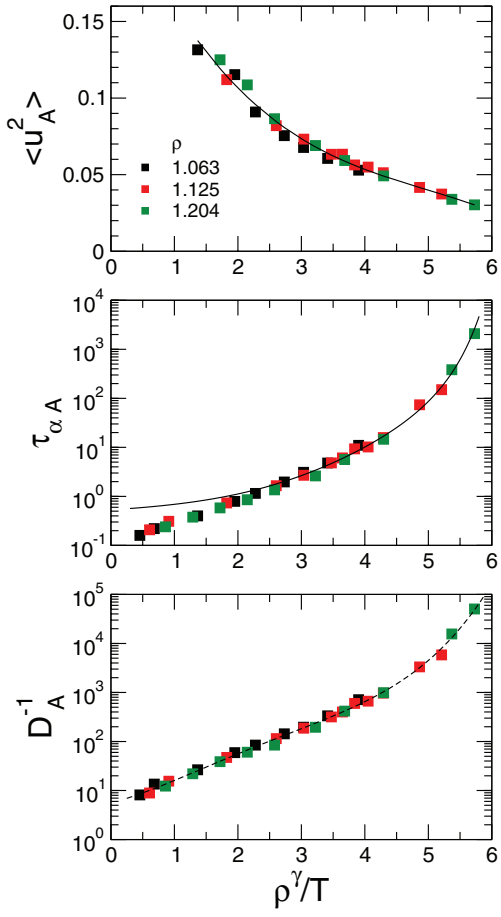

FIG. 8. Thermodynamic scaling of ST-MSD (top), structural relaxation time (middle), and diffusion coefficient (bottom) of the A component of all the states of Fig. 5 with Lennard-Jones potential. $\gamma = 5.1$. The continuous line in the top panel is a polynomial best-fit function. The latter is combined with Eq. (1) with $\overline{a_A^2}$ and $\sigma_{a_A^2}$ as in Table I to lead, with no adjustable parameters, to the continuous line in the middle panel. It is known that Eq. (1) fails for $\tau_\alpha \lesssim 1$.[32,33] The dashed line in the bottom panel is a guide for the eyes.

V. CONCLUSIONS

In this article we have studied by means of extensive molecular-dynamics simulations the slow relaxation, the diffusivity, and the fast cage-dynamics of both components of a class of atomic binary mixtures with different interaction potentials. We find, as formerly observed in polymer melts, that the scaling between the slow relaxation/transport and the picosecond rattling motion inside the cage of the first neighbors for both components of particles is a manifestation of a non-trivial property of the incoherent van Hove function, namely that if two states exhibit coinciding incoherent van Hove function on the picosecond timescale, the coincidence is observed at long times too. To emphasize that the scaling is not related to the properties of the system close to the glass transition, we propose a novel alternative expression of the reduced ST-MSD $\widehat{\langle u^2 \rangle}$, with respect to the original formulation using the ST-MSD at the glass transition. A major result of the present study is that the correlation plot between the diffusivity of the two components of the binary mixtures and their respective reduced ST-MSD, collapse on the same master curve (Fig. 5). This holds true also for the structural relaxation of the two components and the unique master curve coincides with the one of the *average* scaling Eq. (3). We evidenced, as a further example of the predictive strength of the reduced ST-MSD $\widehat{\langle u^2 \rangle}$, that the breakdown of the Stokes-Einstein law exhibited by the distinct atomic species of the mixture and the monomers of a chain in a polymer melt occurs at the *same* $\widehat{\langle u^2 \rangle}$ value. Finally, we find that ST-MSD exhibits the temperature-density thermodynamic scaling. This result: (i) provides a way, in combination with the scaling between the slow relaxation/transport and ST-MSD, to account for the thermodynamic scaling of both the transport and the relaxation of the mixture; (ii) suggests that the thermodynamic scaling is rooted in the fast dynamics.

Note added in proof: Very recently Eq. (1) led to consistent results when tested on ultrastable glasses with structural relaxation times which are 10^{24} times the value for the ordinary glass.[66]

ACKNOWLEDGMENTS

Computational resources by "Laboratorio per il Calcolo Scientifico" (Physics Department, University of Pisa) are gratefully acknowledged. C.D.M. acknowledges support from ERC-226207-PATCHYCOLLOIDS.

APPENDIX: DETAILS ABOUT EQ. (1)

Equation (1) generalizes previous results by Hall and Wolynes relating the structural relaxation time and ST-MSD[8]

$$\tau_\alpha^{(HW)}(a^2) \propto \exp\left(\frac{a^2}{2\langle u^2\rangle}\right), \tag{A1}$$

where a is the displacement to reach the transition state. It is natural to take that the variable a is distributed. In particular, we assume that $p(a^2)$ has a truncated gaussian form[32,33]

$$p(a^2) = \begin{cases} A\exp\left(-\frac{(a^2-\overline{a^2})^2}{2\sigma_{a^2}^2}\right), & \text{if } a > a_{min}, \\ 0, & \text{otherwise}, \end{cases} \tag{A2}$$

where A is the normalization and a_{min}^2 is the minimum square displacement to reach the transition state. A convenient choice is $a_{min}^2 = 0$.[33] By defining

$$\tau_\alpha = \int_0^\infty da^2\, p(a^2)\, \tau_\alpha^{(HW)}(a^2) \tag{A3}$$

one recovers Eq. (1).[33]

Extensive numerical simulations of a model polymer system yield the following best-fit values of the parameters τ_0, $\overline{a^2}$, and $\sigma_{a^2}^2$ of Eq. (1) in MD units[32,33]

$$\tau_0 = 0.377, \tag{A4}$$

$$\overline{a^2} = 0.124, \tag{A5}$$

$$\sigma_{a^2} = 0.251, \tag{A6}$$

leading to Eq. (2).

It must be pointed out that $\overline{a^2}$ and $\sigma_{a^2}^2$ do *not* coincide with the average $E[a^2]$ and the variance $Var[a^2]$ of the distribution $p(a^2)$, respectively. This is due to the truncation and the fact that the best-fit values of $\overline{a^2}$ and σ_{a^2} are comparable. One finds

$$E[a^2] = 0.252, \tag{A7}$$

$$\sqrt{Var[a^2]} = 0.175. \tag{A8}$$

We now show that $E[a^2]$ and $Var[a^2]$ do not rely largely on the form of $p(a^2)$ Eq. (A2) and the numerical simulations. To this aim, we consider a toy model of the barrier crossing in a liquid. Let us refer to Fig. 9. The grey particle, with unit diameter, initially touches two other particles spaced by $2x$. To proceed, the grey particle must overcome the barrier due to the two particles. It must displace a to reach the transition point located on the line joining the centers of the two other particles. The latter, due to the motion of the grey particle, are pushed aside and move along the line joining their initial positions. Assuming that the a-distribution is flat between $0 \le a \le \sqrt{1-x^2}$ one finds

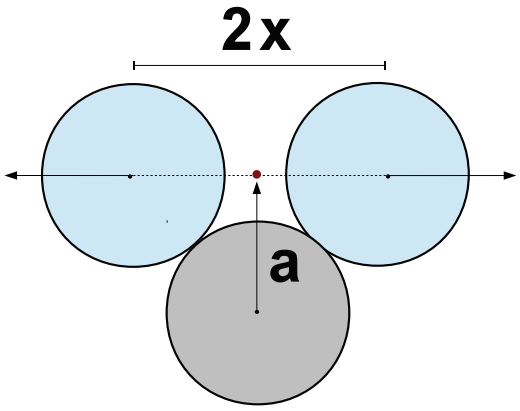

FIG. 9. Toy model of the barrier crossing in a liquid. The grey particle overcomes the barrier due to the blue particles by displacing them along the line joining their centers and reaching the transition point (red dot). Initially, the blue particles are at distance $2x$ apart from each other and the grey particle is at distance a from the transition point. All the particles have unit diameter.

$$E^\star[a^2](x) = (1-x^2)/3, \tag{A9}$$

$$\sqrt{Var^\star[a^2](x)} = 2\sqrt{5}(1-x^2)/15. \tag{A10}$$

If the blue spheres are initially at the equilibrium distance of the A particles ($x = 1/2\,\sigma_{AA}^* = 0.56$), one yields

$$E^\star[a^2](0.56) = 0.229, \tag{A11}$$

$$\sqrt{Var^\star[a^2](0.56)} = 0.205. \tag{A12}$$

The above quantities differ from Eqs. (A7) and (A8) by an error of about 9% and 17%, respectively. Since the model is extremely rough, much more insight into the process leading to the barrier crossing is needed to reach a quantitative understanding of $E[a^2]$ and $Var[a^2]$.

[1] M. D. Ediger and P. Harrowell, J. Chem. Phys. **137**, 080901 (2012).
[2] C. A. Angell, K. L. Ngai, G. B. McKenna, P. McMillan, and S. W. Martin, J. Appl. Phys. **88**, 3113 (2000).
[3] P. G. Debenedetti and F. H. Stillinger, Nature (London) **410**, 259 (2001).
[4] R. Richert, J. Phys.: Condens. Matter **14**, R703 (2002).
[5] $\langle u^2\rangle$ is related to the Debye-Waller factor which, assuming harmonicity of thermal motion, takes the form $\exp(-q^2\langle u^2\rangle/3)$, where q is the absolute value of the scattering vector. Surrogates are known.[65]
[6] A. Tobolsky, R. E. Powell, and H. Eyring, in *Frontiers in Chemistry*, Vol. 1, edited by R. E. Burk and O. Grummit (Interscience, New York, 1943), pp. 125–190.
[7] C. A. Angell, Science **267**, 1924 (1995).
[8] R. W. Hall and P. G. Wolynes, J. Chem. Phys. **86**, 2943 (1987).
[9] J. C. Dyre, N. B. Olsen, and T. Christensen, Phys. Rev. B **53**, 2171 (1996).
[10] L.-M. Martinez and C. A. Angell, Nature (London) **410**, 663 (2001).
[11] K. L. Ngai, Philos. Mag. **84**, 1341 (2004).

[12]K. L. Ngai, J. Non-Cryst. Solids **275**, 7 (2000).
[13]D. S. Simmons, M. T. Cicerone, Q. Zhong, M. Tyagic, and J. F. Douglas, Soft Matter **8**, 11455 (2012).
[14]C. A. Angell, J. Am. Ceram. Soc. **51**, 117 (1968).
[15]S. V. Nemilov, Russ. J. Phys. Chem. **42**, 726 (1968).
[16]J. Shao and C. A. Angell, in *Proceedings of the XVIIth International Congress on Glass, Beijing* (Chinese Ceramic Society, 1995), Vol. 1, pp. 311–320.
[17]F. Starr, S. Sastry, J. F. Douglas, and S. Glotzer, Phys. Rev. Lett. **89**, 125501 (2002).
[18]P. Bordat, F. Affouard, M. Descamps, and K. L. Ngai, Phys. Rev. Lett. **93**, 105502 (2004).
[19]A. Widmer-Cooper and P. Harrowell, Phys. Rev. Lett. **96**, 185701 (2006).
[20]H. Zhang, D. J. Srolovitz, J. F. Douglas, and J. A. Warren, Proc. Natl. Acad. Sci. U.S.A. **106**, 7735 (2009).
[21]A. Widmer-Cooper, H. Perry, P. Harrowell, and D. R. Reichman, Nat. Phys. **4**, 711 (2008).
[22]X. Xia and P. G. Wolynes, PNAS **97**, 2990 (2000).
[23]J. Dudowicz, K. F. Freed, and J. F. Douglas, Adv. Chem. Phys. **137**, 125 (2008).
[24]U. Buchenau and R. Zorn, Europhys. Lett. **18**, 523 (1992).
[25]T. Scopigno, G. Ruocco, F. Sette, and G. Monaco, Science **302**, 849 (2003).
[26]A. P. Sokolov, E. Rössler, A. Kisliuk, and D. Quitmann, Phys. Rev. Lett. **71**, 2062 (1993).
[27]U. Buchenau and A. Wischnewski, Phys. Rev. B **70**, 092201 (2004).
[28]V. N. Novikov and A. P. Sokolov, Nature (London) **431**, 961 (2004).
[29]V. N. Novikov, Y. Ding, and A. P. Sokolov, Phys. Rev. E **71**, 061501 (2005).
[30]S. N. Yannopoulos and G. P. Johari, Nature (London) **442**, E7 (2006).
[31]J. C. Dyre, Rev. Mod. Phys. **78**, 953 (2006).
[32]L. Larini, A. Ottochian, C. De Michele, and D. Leporini, Nat. Phys. **4**, 42 (2008).
[33]A. Ottochian, C. De Michele, and D. Leporini, J. Chem. Phys. **131**, 224517 (2009).
[34]A. Ottochian and D. Leporini, Philos. Mag. **91**, 1786 (2011).
[35]A. Ottochian and D. Leporini, J. Non-Cryst. Solids **357**, 298 (2011).
[36]In Refs. 32 and 33 the reduced ST-MSD was defined as $\langle\widetilde{u^2}\rangle = \langle u^2\rangle/\langle u_g^2\rangle$, thus writing Eq. (1) as $\log\tau_\alpha = \alpha + \tilde{\beta}\,/\langle\widetilde{u^2}\rangle + \tilde{\gamma}/\langle\widetilde{u^2}\rangle^2$ with $\tilde{\beta} = 1.62(6)$ and $\tilde{\gamma} = 12.3(1)$. To convert the reduced ST-MSD $\langle\widetilde{u^2}\rangle$ to $\langle\widehat{u^2}\rangle$ and resort to Eq. (3), one notices that $\overline{a^2} = 2\tilde{\beta}\langle u_g^2\rangle \ln 10$ and then $\langle\widehat{u^2}\rangle = (2\tilde{\beta}\ln 10)^{-1}\langle\widetilde{u^2}\rangle$.
[37]C. De Michele, E. Del Gado, and D. Leporini, Soft Matter **7**, 4025 (2011).
[38]F. Puosi and D. Leporini, J. Chem. Phys. **136**, 211101 (2012).
[39]F. Puosi and D. Leporini, J. Chem. Phys. **136**, 041104 (2012).
[40]F. Puosi and D. Leporini, J. Chem. Phys. **136**, 164901 (2012).
[41]A. Ottochian, F. Puosi, C. De Michele, and D. Leporini, "Comment on 'Generalized localization model of relaxation in glass-forming liquids'," Soft Matter (unpublished).
[42]P. A. Egelstaff, *An Introduction to the Liquid State*, 2nd ed. (Clarendon, Oxford, 1992).
[43]J. P. Hansen and I. R. McDonald, *Theory of Simple Liquids*, 3rd ed. (Academic, 2006).
[44]F. Puosi and D. Leporini, J. Phys. Chem. B **115**, 14046 (2011).
[45]M. D. Ediger, Annu. Rev. Phys. Chem. **51**, 99 (2000).
[46]Note that $t^\star$ is one order of magnitude shorter than the times considered in Ref. 19.
[47]P. Chaudhuri, L. Berthier, and W. Kob, Phys. Rev. Lett. **99**, 060604 (2007).
[48]W. Kob and H. C. Andersen, Phys. Rev. E **51**, 4626 (1995).
[49]W. Kob and H. C. Andersen, Phys. Rev. E **52**, 4134 (1995).
[50]W. Kob and H. C. Andersen, Phys. Rev. Lett. **73**, 1376 (1994).
[51]S. S. Ashwin and S. Sastry, J. Phys.: Condens. Matter **15**, S1253 (2003).
[52]S. Nosé, J. Chem. Phys. **81**, 511 (1984).
[53]M. P. Allen and D. J. Tildesley, *Computer Simulations of Liquids* (Oxford University Press, Clarendon, 1987).
[54]B. Vorselaars, A. V. Lyulin, K. Karatasos, and M. A. J. Michels, Phys. Rev. E **75**, 011504 (2007).
[55]In Ref. 38 the SE breakdown of the polymer system has been investigated in terms of the quantity $R = \Lambda^2/(4\langle\widehat{u_P^2}\rangle)$.
[56]R. Yamamoto and A. Onuki, Phys. Rev. Lett. **81**, 4915 (1998).
[57]F. Mezei, W. Knaak, and B. Farago, Phys. Rev. Lett. **58**, 571 (1987).
[58]C. De Michele and D. Leporini, Phys. Rev. E **63**, 036701 (2001).
[59]S.-H. Chong and W. Kob, Phys. Rev. Lett. **102**, 025702 (2009).
[60]C. M. Roland, S. Hensel-Bielowka, M. Paluch, and R. Casalini, Rep. Prog. Phys. **68**, 1405 (2005).
[61]D. Coslovich and C. M. Roland, J. Phys. Chem. B **112**, 1329 (2008).
[62]D. Coslovich and C. M. Roland, J. Chem. Phys. **131**, 151103 (2009).
[63]M. C. C. Ribeiro, T. Scopigno, and G. Ruocco, J. Chem. Phys. **135**, 164510 (2011).
[64]O. Chulkin, Ph.D. dissertation, Graduate School of Basic Sciences "Galileo Galilei" Applied Physics, Universita' di Pisa, 2011.
[65]M. T. Cicerone, Q. Zhong, J. Johnson, K. A. Aamer, and M. Tyagi, J. Phys. Chem. Lett. **2**, 1464 (2011).
[66]S. Singh, M. D. Ediger, and J. J. de Pablo, Nature Mat. **12**, 139 (2013).